AMERICAN SOCIETY FOR MICROBIOLOGY | Journal of Virology®

GENOME REPLICATION AND REGULATION OF VIRAL GENE EXPRESSION

In Vitro Double-Stranded RNA Synthesis by Rotavirus Polymerase Mutants with Lesions at Core Shell Contact Sites

Courtney L. Steger,[a] Mackenzie L. Brown,[b] Owen M. Sullivan,[b] Crystal E. Boudreaux,[c] Courtney A. Cohen,[d] Leslie E. W. LaConte,[e] Sarah M. McDonald[b]

[a]Translational Biology, Medicine, and Health Graduate Program, Virginia Tech, Blacksburg, Virginia, USA
[b]Department of Biology, Wake Forest University, Winston Salem, North Carolina, USA
[c]West Virginia School of Osteopathic Medicine, Lewisburg, West Virginia, USA
[d]U.S. Army Medical Research Institute for Infectious Diseases, Frederick, Maryland, USA
[e]Fralin Biomedical Research Institute, Roanoke, Virginia, USA

ABSTRACT The rotavirus polymerase VP1 mediates all stages of viral RNA synthesis within the confines of subviral particles and while associated with the core shell protein VP2. Transcription (positive-strand RNA [+RNA] synthesis) by VP1 occurs within double-layered particles (DLPs), while genome replication (double-stranded RNA [dsRNA] synthesis) by VP1 occurs within assembly intermediates. VP2 is critical for VP1 enzymatic activity; yet, the mechanism by which the core shell protein triggers polymerase function remains poorly understood. Structural analyses of transcriptionally competent DLPs show that VP1 is located beneath the VP2 core shell and sits slightly off-center from each of the icosahedral 5-fold axes. In this position, the polymerase is contacted by the core shell at 5 distinct surface-exposed sites, comprising VP1 residues 264 to 267, 547 to 550, 614 to 620, 968 to 980, and 1022 to 1025. Here, we sought to test the functional significance of these VP2 contact sites on VP1 with regard to polymerase activity. We engineered 19 recombinant VP1 (rVP1) proteins that contained single- or multipoint alanine mutations within each individual contact site and assayed them for the capacity to synthesize dsRNA *in vitro* in the presence of rVP2. Three rVP1 mutants (E265A/L267A, R614A, and D971A/S978A/I980A) exhibited diminished *in vitro* dsRNA synthesis. Despite their loss-of-function phenotypes, the mutants did not show major structural changes *in silico,* and they maintained their overall capacity to bind rVP2 *in vitro* via their non-mutated contact sites. These results move us toward a mechanistic understanding of rotavirus replication and identify precise VP2-binding sites on the polymerase surface that are critical for its enzymatic activation.

IMPORTANCE Rotaviruses are important pathogens that cause severe gastroenteritis in the young of many animals. The viral polymerase VP1 mediates all stages of viral RNA synthesis, and it requires the core shell protein VP2 for its enzymatic activity. Yet, there are several gaps in knowledge about how VP2 engages and activates VP1. Here, we probed the functional significance of 5 distinct VP2 contact sites on VP1 that were revealed through previous structural studies. Specifically, we engineered alanine amino acid substitutions within each of the 5 VP1 regions and assayed the mutant polymerases for the capacity to synthesize RNA in the presence of VP2 in a test tube. Our results identified residues within 3 of the VP2 contact sites that are critical for robust polymerase activity. These results are important because they enhance the understanding of a key step of the rotavirus replication cycle.

KEYWORDS RNA synthesis, RNA-dependent RNA polymerase, VP1, VP2, core shell protein, genome replication, rotavirus

Citation Steger CL, Brown ML, Sullivan OM, Boudreaux CE, Cohen CA, LaConte LEW, McDonald SM. 2019. *In vitro* double-stranded RNA synthesis by rotavirus polymerase mutants with lesions at core shell contact sites. J Virol 93:e01049-19. https://doi.org/10.1128/JVI.01049-19.

Editor Susana López, Instituto de Biotecnologia/UNAM

Address correspondence to Sarah M. McDonald, mcdonasm@wfu.edu.

Received 21 June 2019
Accepted 17 July 2019
Accepted manuscript posted online 24 July 2019
Published 30 September 2019

Rotaviruses are segmented, double-stranded RNA (dsRNA) viruses that cause severe gastroenteritis in unvaccinated children and animals (1, 2). The viral RNA-dependent RNA polymerase VP1 catalyzes both the transcription of positive-strand RNAs (+RNAs) and the replication of dsRNA genome segments in a particle-associated manner (3, 4). More specifically, during transcription, VP1 synthesizes +RNAs in the context of double-layered particle (DLPs), which are virions that have shed their outermost layer during entry into the host cell (5, 6). In contrast, genome replication by VP1 occurs in tandem with the early stages of virion particle assembly (3, 7–9). While little structural information exists for replicase-competent assembly intermediates, high-resolution structures of transcriptionally competent DLPs have been solved (10–13). In the DLP, VP1 is detected beneath the innermost T=1 icosahedral VP2 core shell, with a single polymerase monomer positioned just off-center from each of the 5-fold axes (Fig. 1A and B). The core shell itself is composed of 120 copies of VP2 that are arranged as asymmetric dimers, wherein one structural conformer (VP2-A) converges around the 5-fold axes, and a different conformer (VP2-B) interdigitates between adjacent VP2-A proteins (Fig. 1A and B). Each VP2 monomer is separated into a principal scaffold domain (amino acids [aa] ~101 to 880) and a flexible N-terminal domain (NTD; aa ~1 to 100), which is not a major component of the T=1 shell and instead protrudes inside the core (11). The principal scaffold domain of 3 individual VP2 monomers of a 5-fold decameric unit (i.e., VP2-A1, VP2-A2, and VP2-B1) makes contacts with VP1 in the DLP (Fig. 1B and C) (12, 13). The VP2 NTD is not fully structurally resolved, but it is known to engage VP1 and likely helps secure the polymerase against the principal scaffold domain (13). Indeed, it is largely thought that VP1 performs its RNA synthetic processes while it is physically tethered to the VP2 core shell via these contact sites. However, the role of the core shell protein goes beyond merely serving as a physical framework upon which the polymerase functions. The capacity of VP1 to synthesize RNA, *in vitro* and *in vivo*, is dependent upon the presence of VP2, suggesting that the core shell protein is also a critical enzymatic activator of the polymerase (7–9, 14–20). However, the precise contact sites between VP1 and VP2 that culminate in polymerase activation and particle-associated RNA synthesis are poorly understood.

Core shell-dependent dsRNA synthesis, but not +RNA synthesis, by the rotavirus polymerase can be recapitulated *in vitro* using baculovirus-expressed, recombinant (r) proteins (14–19). rVP1 is expressed as a soluble, C-terminally hexahistidine-tagged protein in *Spodoptera frugiperda* (Sf9) cells and purified using metal affinity chromatography (14–19). The rVP2 core shell protein is untagged and insoluble following Sf9 cell expression because of its intrinsic capacity to multimerize in solution and form various high-molecular-weight assembly intermediates (21). Importantly, rVP1 will synthesize dsRNA from a viral +RNA template *in vitro*, but only when multimeric rVP2 is added to the reaction (14–19). Our previous work has demonstrated that activation of rVP1 by rVP2 is specific, such that different rotavirus strains can encode noncompatible proteins (17–19). For example, group A strain SA11 rVP1 is activated by cognate SA11 rVP2 but not by noncognate group C strain Bristol rVP2 and vice versa (i.e., strain Bristol rVP1 is activated by Bristol rVP2 but not by strain SA11 rVP2) (17). Likewise, group A avian and simian rVP1 and rVP2 (strains PO-13 and SA11) are not cross-compatible (18, 19). Chimeric mutagenesis of rVP2 demonstrated that the specificity of rVP1 activation maps to the principal scaffold domain (aa 100 to 700 and 830 to 880) and not the NTD as was previously predicted (18). Nevertheless, the rVP2 NTD also plays an important role in polymerase activation, likely by securing rVP1 against the principal scaffold domain (18). Indeed, deletion of the NTD renders rVP2 unable to robustly activate rVP1 *in vitro* (18).

The structure of rVP1 has been solved to atomic resolution, revealing a globular, cage-like enzyme of 1,089 amino acids (aa) in length (22). VP1 is composed of an amino-terminal domain (NTD; aa 1 to 332), a central right-handed polymerase domain (PD; aa 333 to 778), and a carboxy-terminal domain (CTD; aa 779 to 1089) (Fig. 2A). The PD is structurally and functionally conserved across diverse viral RNA-dependent RNA polymerases, and it contains several orthologous subdomains (fingers, palm, and

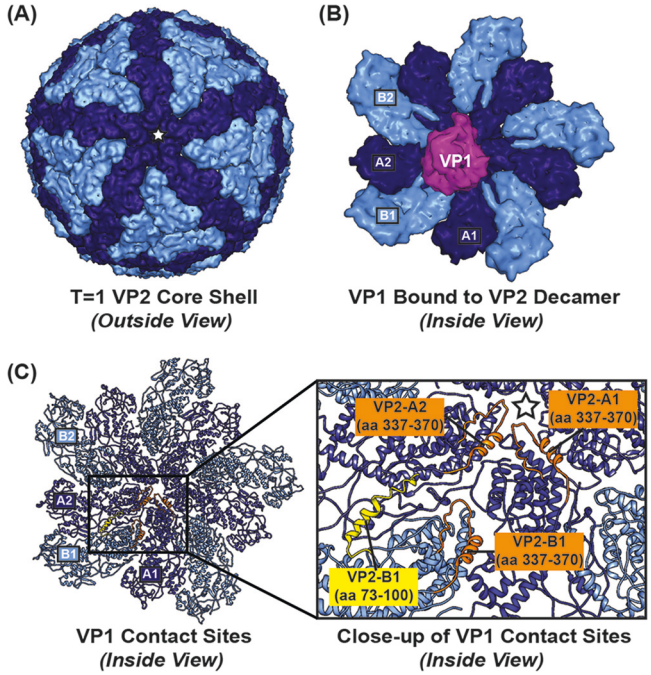

FIG 1 DLP structure of the rotavirus VP2 core shell and position of the VP1 polymerase. (A) Surface rendering of the VP2 core shell in the context of the DLP (PDB accession no. 4F5X), viewed from outside the particle into an icosahedral 5-fold axis (star). Each 5-fold axis is tightly encircled by five copies of VP2-A conformers (dark blue), while five VP2-B conformers (light blue) intercalate between VP2-A. Twelve decameric units of VP2 surround each 5-fold axis and comprise the innermost core shell. (B) Internal view of a 5-fold decameric unit, represented in surface fill with colors for VP2-A and VP2-B as in panel A. Multiple individual VP2 monomers (e.g., A1, A2, and B1) of the decamer contact a single VP1 monomer (magenta) positioned below the core shell just off-center from the 5-fold axis, which is obscured by VP1 in this image. (C) Ribbon representation of the VP2 decamer shown in panel B is shown on the left. For clarity, the VP1 monomer has been removed. A black box outlines the area that is magnified in the image on the right. Regions of VP2 that contact VP1 in the DLP are highlighted in orange (aa 337 to 370) or bright yellow (aa 73 to 100) for three distinct VP2 monomers (A1, A2, and B1). The 5-fold axis is represented by a star, as in panel A.

thumb) and motif elements (motifs A to F) (22–24). The active site is buried within the hollow center of the globular enzyme, and it is composed of invariant Glu-Asp-Asp residues of the PD (22–24). Four tunnels permeate VP1 and allow for the entry of single-stranded RNA templates, the entry of nucleoside triphosphates (NTPs) and divalent metal cations, the exit of +RNA transcripts, and the exit of newly formed dsRNA genome segments (Fig. 2B and C) (22). In the high-resolution structures of the DLP (i.e., the transcriptase complex), VP1 is oriented such that its +RNA exit tunnel presses against the VP2 core shell (12, 13). This position and orientation for the rotavirus polymerase are consistent with those of other *Reoviridae* family members (25, 26). For rotavirus, 5 distinct regions of VP1 overlap the VP2 principal scaffold domain in the DLP structures (12, 13). We refer to these regions of VP1 as core shell protein contact sites C1 to C5. Site C1 is located within the VP1 NTD (aa 264 to 267), while C4 and C5 are located in the VP1 CTD (aa 968 to 980 and 1022 to 1025, respectively) (Fig. 2A and D). C2 is positioned within the fingers subdomain of the PD (aa 547 to 550), whereas C3 is situated in the palm subdomain of the PD (aa 614 to 620) (Fig. 2A and D). On the VP2 side of the interaction, two VP2-A subunits (A1 and A2) and one VP2-B subunit (B1) make contacts with VP1 (Fig. 1C and 2E) (12, 13). The most extensive overlap occurs within a region of VP2 that encompasses aa 337 to 370 within the principal scaffold domain. Still, VP2 NTD residues 73 to 100 of a single VP2-B conformer (B1) converge toward VP1 site C1 in the DLP structure (Fig. 1C and 2E). Additional contacts between the VP2 NTD were revealed in the transcribing DLP structure; these flexible tethers are wrapped around the sides of VP1 (13).

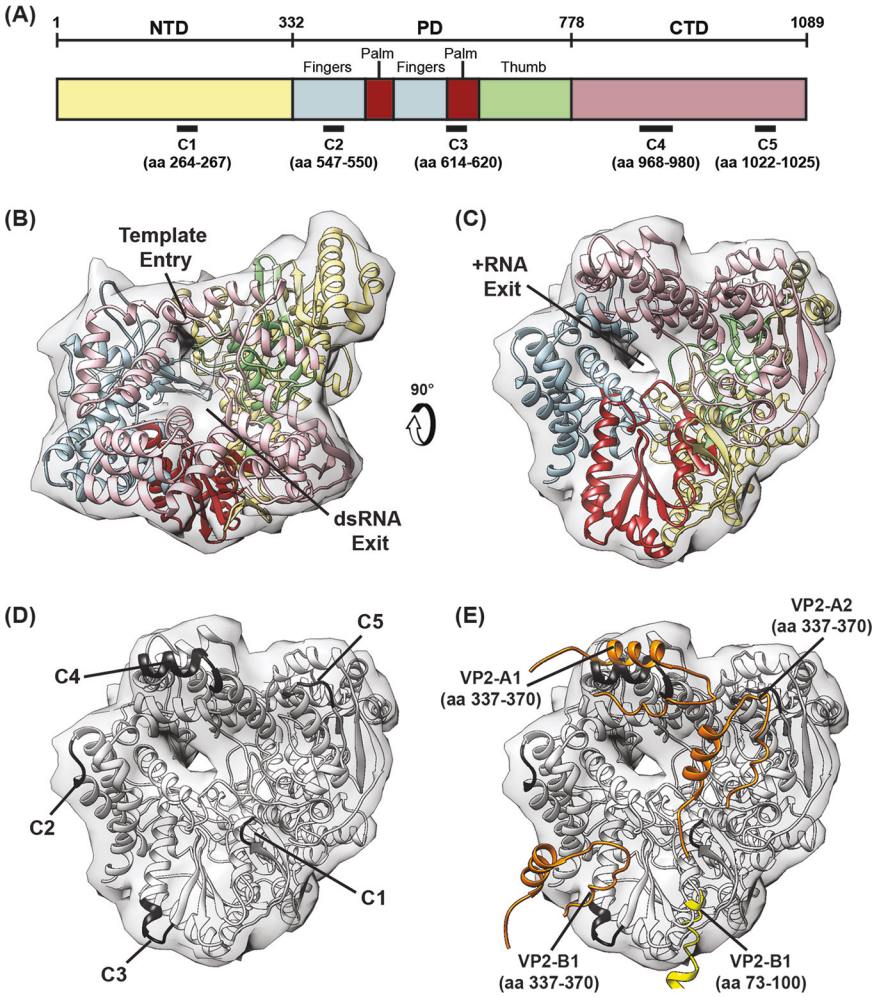

FIG 2 Structure of the VP1 polymerase and sites of contact with the VP2 core shell. (A) VP1 is shown as a linear schematic and colored according to domain/subdomain organization, with amino acid residues of domain interfaces labeled above the gene. The N-terminal domain (NTD; light yellow) and C-terminal domain (CTD; pink) flank the central polymerase domain (PD), which is composed of canonical finger (blue), palm (red), and thumb (green) subdomains. Regions of VP1 that contact VP2 in the DLP are labeled with a black bar below the corresponding region of schematic. These contact regions are labeled C1 to C5. (B) Conventional orientation of the VP1 enzyme (PDB accession no. 4AU6 and 4F5X) shown in ribbon representation and colored according to domain organization depicted in panel A, with transparent surface fill outlined in gray. Known or putative functions of two VP1 tunnels that traverse into the catalytic center are labeled. (C) Image in panel B rotated 90° backward to show the surface of VP1 surrounding the +RNA exit tunnel, which borders VP2 within the DLP. (D) Structure in panel C shown in grayscale, with VP1-VP2 contact sites on VP1 (C1 to C5) colored in black and listed on the image. (E) Structure in panel D with VP1-VP2 contact sites on three VP2 monomers (A1, A2, and B1) shown in ribbon representation and colored as in Fig. 1C. For clarity, all other regions of VP2 have been removed.

While VP2 clearly engages VP1 at numerous contact sites, we hypothesize that only a small number of residues within some of these sites function to trigger conformational changes that activate the enzyme. In the current study, we sought to probe the functional importance of the 5 VP2 principal scaffold domain contact sites located on the VP1 +RNA exit tunnel interface (i.e., C1 to C5) that were identified in the DLP structures (12, 13). We employed alanine mutagenesis of group A simian strain SA11 rVP1 and assayed mutant polymerase activity, compared to the wild-type (WT) control rVP1, in the presence of SA11 rVP2 using the *in vitro* dsRNA synthesis assay. Our results showed that alanine mutations at some residues in regions C1, C3, and C4 reduced the capacity of rVP1 to synthesize dsRNA in the presence of rVP2. More specifically, one single-point mutant in C2 (R614A) and two multipoint mutants in C1 (E265A/L267A) and C4 (D971A/S978A/I980A) showed decreased *in vitro* dsRNA synthesis. As expected,

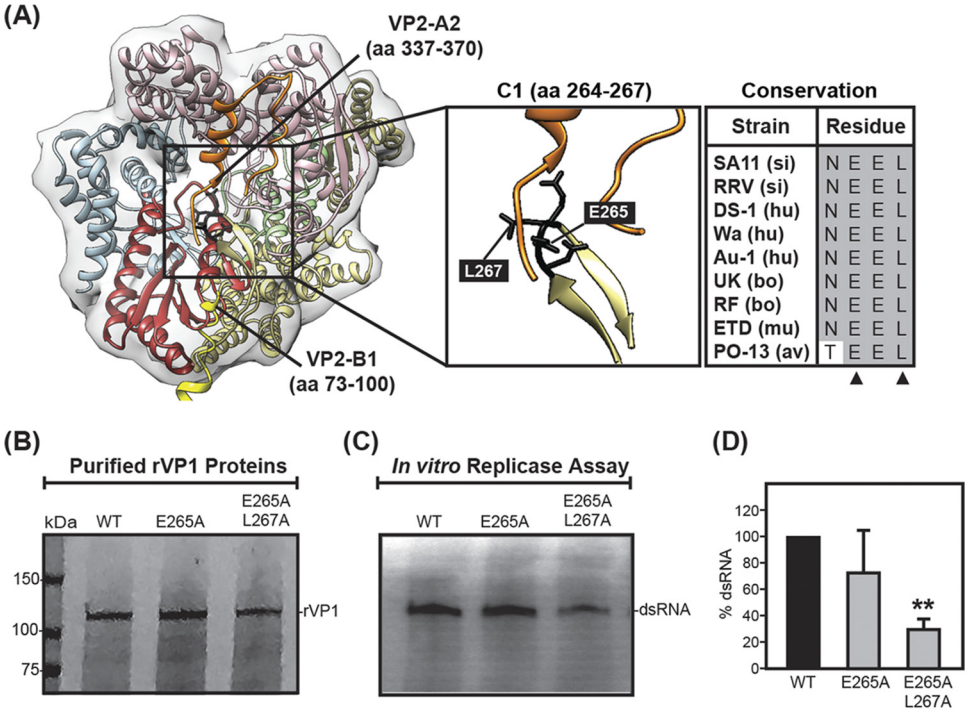

FIG 3 *In vitro* dsRNA synthesis by rVP1 C1 alanine mutants. (A) A ribbon representation of VP1 (PDB accession no. 4AU6 and 4F5X) is shown on the left in the same orientation and coloration as in Fig. 2C. Ribbon representations of VP2-A2 (aa 337 to 370; orange) and VP2-B1 (aa 73 to 100; yellow) are shown in the image on the left in the same orientation and coloration as in Fig. 2E. A black box outlines the area of C1 (aa 264 to 267, NEEL) that is magnified in the image on the right. For clarity, some regions of VP1 and VP2 have been removed. C1 is colored black, and residues mutated in this study are shown in stick representations and labeled. Amino acid sequence conservation for C1 is shown as an alignment in which strain name is listed to the left, with species of origin in parentheses as follows: simian, si; human, hu; bovine, bo; murine, mu; and avian, av. Gray shading indicates conservation of amino acid identity, and variable amino acid residues are highlighted in white. (B) Approximately 2 pmol purified WT SA11 rVP1 or point mutant rVP1 was electrophoresed on a 10% SDS-polyacrylamide gel and visualized by Coomassie blue stain. A molecular mass (in kilodaltons) marker is shown to the left. (C) Radiolabeled dsRNA synthesis products were synthesized by 2 pmol each rVP1 in the presence of 8 pmol rVP2 from strain SA11 rVP2. All reaction mixtures contained 8 pmol +RNA template and were incubated at 37°C for 180 min. Radiolabeled dsRNA products were resolved on 10% SDS-polyacrylamide gels and visualized using a phosphorimager. (D) Radiolabeled dsRNA was quantified. The results are means from 6 independent experiments using at least 3 protein batches normalized to the WT (100%). Error bars represent standard deviations from the mean. A double asterisk indicates a *P* value of <0.001.

the loss-of-function alanine mutations did not ablate the overall capacity of the rVP1 proteins to interact with rVP2 via nonmutated sites, as measured by pulldown and virus-like particle encapsidation assays. *In silico* molecular dynamics simulations revealed that these alanine mutants of rVP1 are predicted to be properly folded, with no major changes seen in the catalytic site or in template-binding residues. These results are consistent with the hypothesis that subtle contacts by the core shell protein principal scaffold domain at residues within C1, C3, and C4 may trigger enzymatic activation of the rotavirus polymerase.

RESULTS

Simultaneous mutation of rVP1 C1 residues E265 and L267 diminishes *in vitro* dsRNA synthesis. Site C1 (strain SA11 VP1 aa 264 to 267; NEEL) is located in the VP1 NTD, and it contains two consecutive, negatively charged glutamic acid residues that are flanked on either side by a polar residue (Fig. 3A). In general, these residues are conserved among group A rotavirus strains, with the exception of asparagine at position 264, which is threonine in some avian strains (Fig. 3A). The glutamic acid side chain at position 265 is both surface exposed and points outwards toward the VP2 core shell, making contacts with aa 337 to 339 of a single VP2-A2 monomer (Fig. 3A) (12, 13). The structurally resolved portion of the VP2 NTD from a neighboring VP2-B1 monomer (aa

73 to 100) also protrudes toward C1 and is predicted to clash with the polymerase at/near this site (Fig. 3A) (12, 13). To investigate the significance of residues within C1 on VP2-dependent VP1 polymerase activity, we engineered single- and double-alanine mutations at positions 265 and/or 267 (i.e., E265A and E265A/L267A) in the backbone of simian strain SA11 rVP1. The E265A, E265A/L267A, and WT rVP1 proteins were expressed in Sf9 cells, purified by metal affinity chromatography, and visualized following sodium dodecyl sulfate-polyacrylamide gel electrophoresis (SDS-PAGE) and Coomassie blue staining (Fig. 3B). The rVP1 proteins were then assayed for their capacity to synthesize dsRNA *in vitro* in reaction mixtures containing SA11 rVP2, SA11 +RNA gene 8 template, divalent cations, NTPs, and trace amounts of [^{32}P]UTP. The newly synthesized ^{32}P-labeled dsRNA products of the reactions were resolved by SDS-PAGE and then visualized/quantified using a phosphorimager (Fig. 3C and D). The results showed that E265A rVP1 synthesized dsRNA at levels that were indistinguishable from those of WT rVP1. However, the E265A/L267A rVP1 double-alanine mutant synthesized significantly reduced levels of the dsRNA product, yielding only ~25% of the WT levels (Fig. 3D). These results indicate that mutating the highly conserved, surface-exposed, electrically charged glutamic acid residue to a hydrophobic alanine residue alone was not sufficient to abrogate rVP2 interactions and/or diminish the enzymatic activity of rVP1. However, combining this E265A mutation with another more modest leucine-to-alanine change at position 267 (i.e., L267A) was sufficient to diminish the *in vitro* enzymatic activity of rVP1.

Mutation of individual rVP1 C2 residues has no effect on *in vitro* dsRNA synthesis. Site C2 (strain SA11 VP1 aa 547 to 550; NMTN) is located in the fingers subdomain of the PD, and it maintains highly conserved amino acid chemistry at each position (Fig. 4A). In particular, this region contains three polar residues (N547, T549, and N550) and one hydrophobic residue (M548) in the middle (Fig. 4A). The asparagine at position 547 is conserved among most group A strains but can be threonine in some avian and/or murine strains (Fig. 4A). Also, some murine strains show a unique methionine-to-leucine mutation at position 548 (Fig. 4A). Residues M548 and N550 have side chains that are pointed toward the VP2 core shell in the DLP structure, specifically toward aa 373 to 370 of VP2-B1, though they do not directly clash with any of the VP2 monomers (Fig. 4A) (12, 13). To investigate whether these C2 residues were critical for VP2-dependent VP1 polymerase activity, we engineered and purified rVP1 mutants with individual alanine mutations at each position (i.e., N547A, M548A, T549A, and N550A) (Fig. 4B). Our rationale for making only single-alanine mutations was that this region lies in a subdomain that is important for +RNA template recognition and catalysis; multiple mutations in this region would be expected to negatively impact the enzymatic activity of the polymerase in a manner that is independent of VP2 contact. Indeed, previous studies showed that single-alanine mutations of non-surface-exposed finger subdomain residues K420, R451, R452, R457, R458, R460, I461, I462, and K594 significantly diminished rVP1 polymerase activity *in vitro* (27, 28). Therefore, we were somewhat surprised to find that the *in vitro* dsRNA levels produced by C2 rVP1 N547A, M548A, T549A, and N550A mutants were comparable to those of WT rVP1 (Fig. 4C and D). This result suggests that, individually, the uncharged polar or hydrophobic amino acid side chains within C2 are not critical for enzyme functionality during *in vitro* dsRNA synthesis.

Mutation of rVP1 C3 residue R614 alone reduces *in vitro* dsRNA synthesis. Site C3 (strain SA11 VP1 aa 614 to 620; RISNKHS) is located within the palm subdomain (motif B) of the PD, and it contains two electrically charged residues (i.e., R614 and K618), two hydrophobic residues (i.e., I615 and Y619), one highly conserved polar residue (i.e., N617), and several positions that accommodate variable amino acid chemical propensities (Fig. 5A). Most strikingly, position 618 contains a positively charged lysine in most strains but adopts a negatively charged glutamic acid residue in a murine ETD strain (Fig. 5A). Additionally, the highly conserved hydrophobic tyrosine residue at position 619 is a positively charged histidine residue in simian strain SA11,

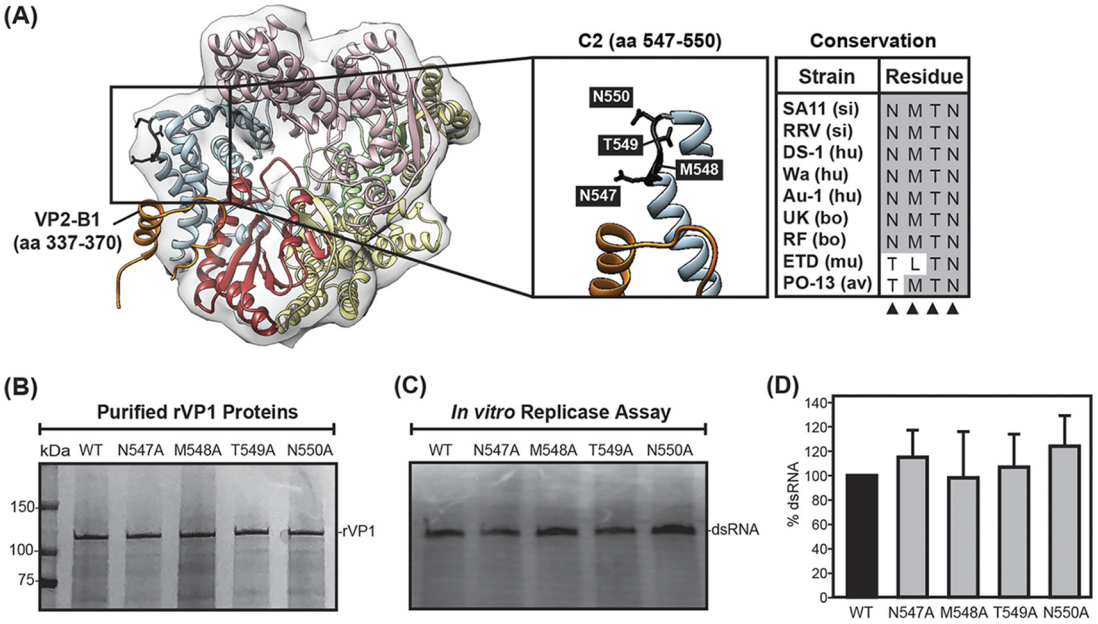

FIG 4 *In vitro* dsRNA synthesis by rVP1 C2 alanine mutants. (A) A ribbon representation of VP1 (PDB accession no. 4AU6 and 4F5X) is shown on the left in the same orientation and coloration as in Fig. 2C. A ribbon representation of VP2-B1 (aa 337 to 370) is shown in the image on the left in the same orientation and coloration as in Fig. 2E. A black box outlines the area of C2 (aa 547 to 550, NMTN) that is magnified in the image on the right. For clarity, some regions of VP1 and VP2 have been removed. C2 is colored black, and residues mutated in this study are shown in stick representations and labeled. Amino acid sequence conservation for C2 is shown as an alignment in which strain name is listed to the left, with species of origin in parentheses as follows: simian, si; human, hu; bovine, bo; murine, mu; and avian, av. Gray shading indicates conservation of amino acid identity, and variable amino acid residues are highlighted in white. (B) Approximately 2 pmol purified WT SA11 rVP1 or point mutant rVP1 was electrophoresed on a 10% SDS-polyacrylamide gel and visualized by Coomassie blue stain. A molecular mass (in kilodaltons) marker is shown to the left. (C) Radiolabeled dsRNA synthesis products were synthesized by 2 pmol each rVP1 in the presence of 8 pmol rVP2 from strain SA11 rVP2. All reaction mixtures contained 8 pmol +RNA template and were incubated at 37°C for 180 min. Radiolabeled dsRNA products were resolved on 10% SDS-polyacrylamide gels and visualized using a phosphorimager. (D) Radiolabeled dsRNA quantified. The results are means from 4 independent experiments using at least 3 protein batches and are normalized to the WT (100%). Error bars represent standard deviations from the mean.

thereby altering the chemical properties of the residue but maintaining the bulky ring structure in the amino acid side chain (Fig. 5A). Residues at positions 616 and 620 are not conserved; rather, they toggle between polar uncharged serine residues or a hydrophobic alanine residue for various rotavirus strains (Fig. 5A). Site C3 contains some residues with electrically charged side chains that are directed outwards toward the VP2 core shell, such as R614 and K618 (Fig. 5A). C3 residues are located adjacent to the loop-helix-loop regions of VP2-B1 (aa 373 to 370) in the DLP (Fig. 5A). To investigate whether these C3 residues were important for VP2-dependent VP1 polymerase activity, we engineered rVP1 mutants with mutations at these positions (i.e., R614A, N617A, K618A, and S616A/S620A). Since C3 is located within the palm subdomain and neighbors the buried active site (strain SA11 aa residues 630 to 632), we again reasoned that multiple mutations in this region could inhibit enzymatic activity in a VP2-independent manner (e.g., local conformational changes that disrupt the active site). Specifically, a previous study showed that alanine mutations in the palm domain (motifs A, C, and priming loop) can ablate the capacity of rVP1 to synthesize dsRNA *in vitro* (28). Thus, we again only engineered single-point mutants in this PD region, with the exception of positions S616 and S620, which already showed an evolutionary tolerance for alanine residues. The rVP1 point mutants were expressed and purified alongside the WT rVP1 control protein and assayed for *in vitro* dsRNA synthesis (Fig. 5B and C). The results showed that dsRNA levels produced by the mutants were comparable to those of WT rVP1, with the exception of R614A rVP1. This single-alanine mutant produced dsRNA at levels that were only ~50% of that in the WT rVP1 (Fig. 5C and D). These results suggest that mutating a highly conserved, surface-exposed, electrically charged arginine amino

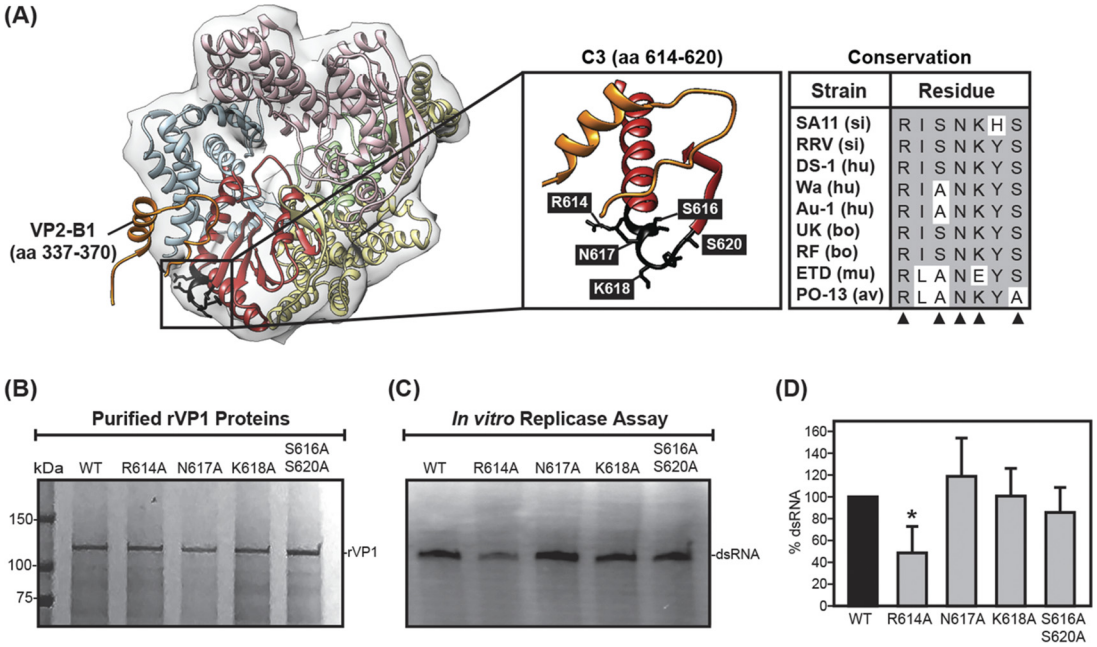

FIG 5 *In vitro* dsRNA synthesis by rVP1 C3 alanine mutants. (A) A ribbon representation of VP1 (PDB accession no. 4AU6 and 4F5X) is shown on the left in the same orientation and coloration as in Fig. 2C. A ribbon representation of VP2-A2 (aa 337 to 370; orange) is shown in the image on the left in the same orientation and coloration as in Fig. 2E. A black box outlines the area of C3 (aa 614 to 620, RISNKHS) that is magnified in the image on the right. For clarity, some regions of VP1 and VP2 have been removed. C3 is colored black, and residues mutated in this study are shown in stick representations and labeled. Amino acid sequence conservation for C3 is shown as an alignment in which the strain name is listed to the left, with species of origin in parentheses as follows: simian, si; human, hu; bovine, bo; murine, mu; and avian, av. Gray shading indicates conservation of amino acid identity, and variable amino acid residues are highlighted in white. (B) Approximately 2 pmol purified WT SA11 rVP1 or point mutant rVP1 was electrophoresed on a 10% SDS-polyacrylamide gel and visualized by Coomassie blue stain. A molecular mass (in kilodaltons) marker is shown to the left. (C) Radiolabeled dsRNA synthesis products were synthesized by 2 pmol each rVP1 in the presence of 8 pmol rVP2 from strain SA11 rVP2. All reaction mixtures contained 8 pmol +RNA template and were incubated at 37°C for 180 min. Radiolabeled dsRNA products were resolved on 10% SDS-polyacrylamide gels and visualized using a phosphorimager. (D) Radiolabeled dsRNA was quantified. The results are the means from 4 independent experiments using at least 2 protein batches and are normalized to the WT (100%). Error bars represent standard deviations from the mean. A single asterisk indicates a *P* value of <0.005.

acid residue to a hydrophobic alanine residue at position 614 was sufficient to diminish the enzymatic activity of rVP1.

Simultaneous mutation of rVP1 C4 residues D971, S978, and I980 nearly ablates *in vitro* dsRNA synthesis. Site C4 (strain SA11 VP1 aa 968 to 980; PKIDADTY VGSKI) is located in the VP1 CTD, and it directly clashes with aa 340 to 370 of VP2-A1 in the structures of the DLP (Fig. 6A) (12, 13). C4 is the largest of the VP2 contact regions and contains four electrically charged residues (i.e., K969, D971, D973, and K979), two polar residues (i.e., T974 and S978), and many hydrophobic and/or nonpolar residues (Fig. 6A). Interestingly, several positions within C4 show amino acid signatures unique to avian strains, including two residues at positions 969 and 979, which exhibit negatively charged residues in avian strains but maintain either positively charged or nonpolar residues in other rotavirus strains (Fig. 6A). Several residues within C4 have highly conserved identity across all strains (i.e., P968, D971, Y975, S978, and I980), and even more display conserved amino acid similarity (Fig. 6A). Yet, only one residue, that of SA11 VP1 position D971, is both conserved and electrically charged (Fig. 6A). Unfortunately, SA11 rVP1 proteins with a single point mutation substituting D971A were expressed at very low levels in insect cells and could not be purified at levels high enough to test for functional activity in the dsRNA synthesis assay (data not shown). Nonetheless, we generated SA11 rVP1 mutants with single alanine point mutations at conserved positions P968, I970, and S978 and assayed for the capacity to synthesize dsRNA *in vitro* (Fig. 6B and C). The results showed that the mutants produced dsRNA at levels comparable to that in the WT rVP1, suggesting that they were all properly folded,

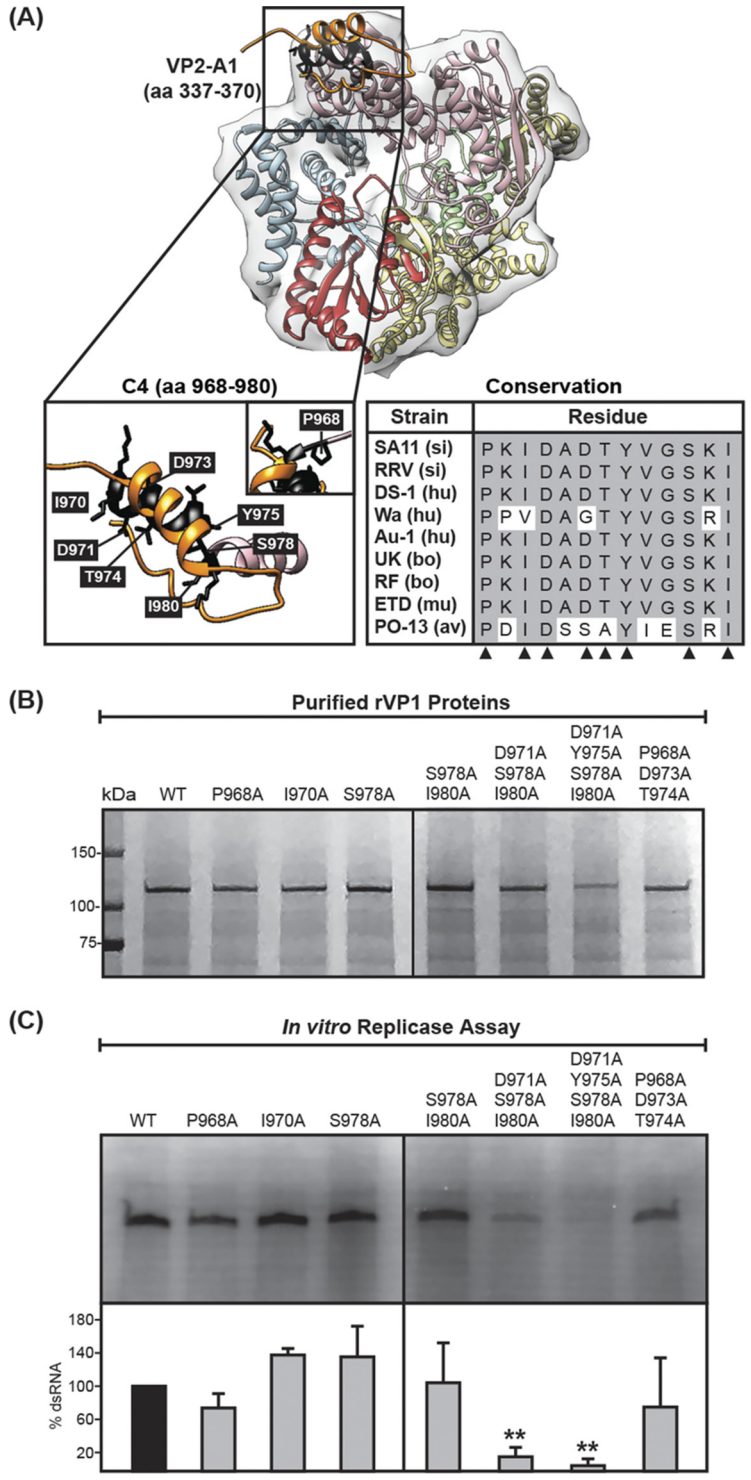

FIG 6 *In vitro* dsRNA synthesis by rVP1 C4 alanine mutants. (A) A ribbon representation of VP1 (PDB accession no. 4AU6 and 4F5X) is shown on the left in the same orientation and coloration as in Fig. 2C. A ribbon representation of VP2-A1 (aa 337 to 370; orange) is shown in the image on the left in the same orientation and coloration as in Fig. 2E. A black box outlines the area of C4 (aa 968 to 980, PKIDADTY VGSKI) that is magnified in the image on the right. For clarity, some regions of VP1 and VP2 have been removed. C4 is colored black, and residues mutated in this study are shown in stick representations and labeled. Amino acid sequence conservation for C4 is shown as an alignment in which strain name is listed to the left, with species of origin in parentheses as follows: simian, si; human, hu; bovine, bo; murine, mu; and avian, av. Gray shading indicates conservation of amino acid identity, and variable amino acid residues are highlighted in white. (B) Approximately 2 pmol purified WT SA11 rVP1 or point mutant rVP1 was electrophoresed on a 10% SDS-polyacrylamide gel and visualized by Coomassie blue stain. A

(Continued on next page)

interacted with rVP2, and were functional under the assay conditions (Fig. 6C and D). These data indicate that, individually, the amino acid side chains of conserved residues within this region are not critical for VP2 interactions or VP1 activity. It is possible that multiple residues within this region engage VP2 in a combinatorial mechanism to induce enzyme activation.

We next generated SA11 rVP1 multipoint mutants wherein 2 to 4 clustered, conserved, and surface-exposed amino acid residues within C4 were switched to alanine (Fig. 6B). We hypothesized that clustered alanine substitutions would diminish the functional capacity of SA11 rVP1 mutants if the changed residues were involved in maintaining enzymatic function via interactions with rVP2. Most of the multipoint mutant rVP1 proteins purified at levels comparable to those of SA11 rVP1 WT, with the exception of the quadruple point mutant (i.e., D971A/Y975A/S978A/I980A), which yielded lower levels of purified protein (Fig. 6B and data not shown). Mutants S978A/I980A rVP1 and P968A/D973A/T974A rVP1 produced dsRNA at levels comparable to those of WT rVP1 (Fig. 6C and D). In contrast, the D971A/S978A/I980A rVP1 mutant showed significantly reduced dsRNA levels compared to those in WT rVP1, yielding only ~20% of the product (Fig. 6C and D). These results suggest that the addition of a D971A mutation in combination with S978A and I980A is sufficient to decrease dsRNA synthesis by rVP1 under the *in vitro* assay conditions. We predict that the electrically charged D971 of C4, with combinatorial effects from surrounding residues, is critical for maintaining functional capacity of rVP1 *in vitro*, possibly by mediating activating interaction(s) with rVP2.

Mutation of rVP1 C5 residues alone or in combination does not affect *in vitro* dsRNA synthesis. Site C5 (strain SA11 VP1 aa 1022 to 1025; FKGK) is located in the VP1 CTD, and all four of its amino acid residues are completely conserved across group A strains (Fig. 7A). C5 contains two positively charged lysine residues with long amino acid side chains that extend toward the VP2 core shell and overlap aa 354 to 370 of VP2-A1 (Fig. 7A). We hypothesized that a multipoint mutant that contained a lysine-to-alanine substitution in combination with other alanine substitutions of surrounding residues would decrease the affinity of intermolecular interactions between rVP1 and rVP2 at this site only, and thus, decrease dsRNA synthesis levels. To test whether double or triple alanine point mutations were sufficient to diminish functional activity of the enzyme, we generated mutants with 2 or 3 alanine substitutions within C5 (Fig. 7B). Surprisingly, all of the rVP1 C5 mutants produced dsRNA at levels indistinguishable from those of WT rVP1 (Fig. 7C and D). These results suggest that C5 is not important for rVP2 interaction(s) that activate rVP1 *in vitro*.

Loss-of-function rVP1 mutants retain overall rVP2-binding capabilities. Our results show that alanine mutagenesis of residues within core shell protein contact sites C1 (E265A/L267A), C3 (R164A), and C4 (D971A/S978A/I980A) reduce the capacity of rVP1 to synthesize dsRNA *in vitro*. Given that the VP2 core shell engages VP1 at several contact sites, we hypothesized that alanine mutation(s) of only 1 to 3 amino acids at a single site (i.e., C1, C3, or C4) would not ablate overall rVP2 binding by rVP1. We tested this hypothesis using two complementary approaches that are amenable to the biochemical nature of multimeric rVP2 (Fig. 8). First, we performed an *in vitro* pulldown assay in which WT or mutant rVP1 proteins were incubated in the presence or absence of rVP2. The mixture was then subjected to centrifugation, which causes the multimeric rVP2 capsid protein to pellet. We expected that rVP1 would be found along with rVP2 in the pellet fraction only if it retained its interaction. The fractionation pattern of rVP1 in the

FIG 6 Legend (Continued)
molecular mass (in kilodaltons) marker is shown to the left. (C) Radiolabeled dsRNA synthesis products were synthesized by 2 pmol each rVP1 in the presence of 8 pmol rVP2 from strain SA11 rVP2. All reaction mixtures contained 8 pmol +RNA template and were incubated at 37°C for 180 min. Radiolabeled dsRNA products were resolved on 10% SDS-polyacrylamide gels and visualized using a phosphorimager. (D) Radiolabeled dsRNA was quantified. The results are means from 6 independent experiments using at least 3 protein batches and are normalized to the WT (100%). Error bars represent standard deviations from the mean. A double asterisk indicates a *P* value of <0.001.

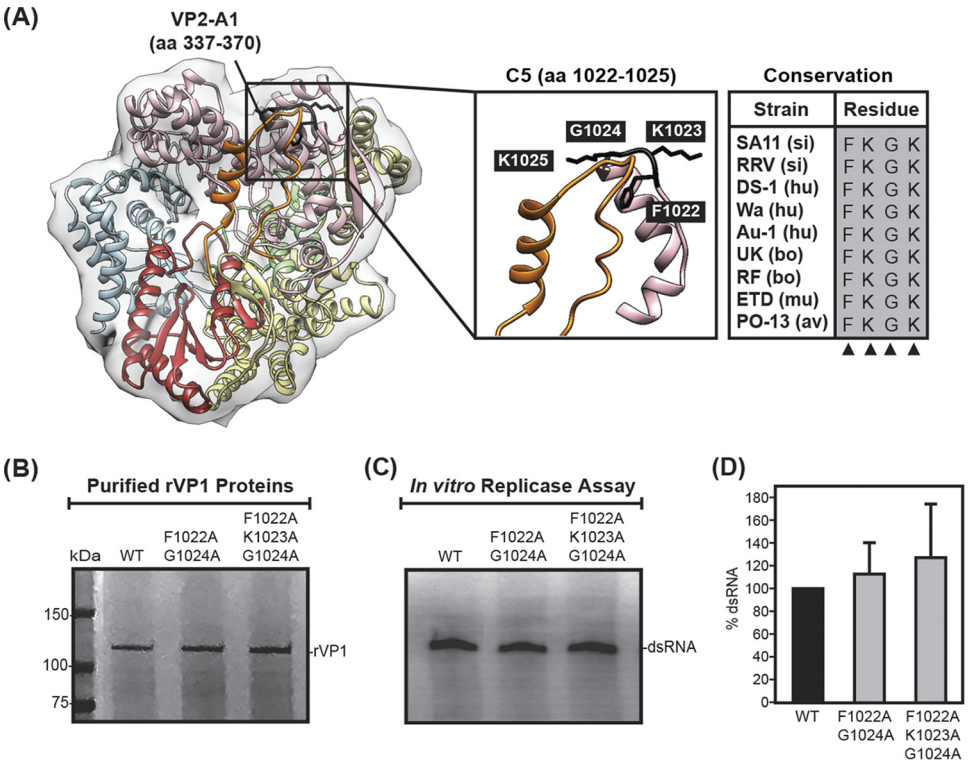

FIG 7 *In vitro* dsRNA synthesis by rVP1 C5 alanine mutants. (A) A ribbon representation of VP1 (PDB accession no. 4AU6 and 4F5X) is shown on the left in the same orientation and coloration as in Fig. 2C. A ribbon representation of VP2-A1 (aa 337 to 370; orange) is shown in the image on the left in the same orientation and coloration as in Fig. 2E. A black box outlines the area of C5 (aa 1022 to 1025, FKGK) that is magnified in the image on the right. For clarity, some regions of VP1 and VP2 have been removed. C5 is colored black, and residues mutated in this study are shown in stick representations and labeled. Amino acid sequence conservation for C5 is shown as an alignment in which strain name is listed to the left, with species of origin in parentheses as follows: simian, si; human, hu; bovine, bo; murine, mu; and avian, av. Gray shading indicates conservation of amino acid identity, and variable amino acid residues are highlighted in white. (B) Approximately 2 pmol purified WT SA11 rVP1 or point mutant rVP1 was electrophoresed on a 10% SDS-polyacrylamide gel and visualized by Coomassie blue stain. A molecular mass (in kilodaltons) marker is shown to the left. (C) Radiolabeled dsRNA synthesis products were synthesized by 2 pmol each rVP1 in the presence of 8 pmol rVP2 from strain SA11 rVP2. All reaction mixtures contained 8 pmol +RNA template and were incubated at 37°C for 180 min. Radiolabeled dsRNA products were resolved on 10% SDS-polyacrylamide gels and visualized using a phosphorimager. (D) Radiolabeled dsRNA was quantified. The results are means from 6 independent experiments using at least 3 protein batches and are normalized to the WT (100%). Error bars represent standard deviations from the mean.

presence versus absence of rVP2 was then assessed following SDS-PAGE and Coomassie blue staining (Fig. 8A and B). The results showed that, in the absence of rVP2, the WT and mutant rVP1 proteins were enriched in the supernatant fraction, with very little (<25%) rVP1 detected in the pellet fraction. In contrast, the WT and mutant rVP1 proteins were all enriched in the pellet fraction (>80%) in the presence of rVP2 at comparable levels (Fig. 8B). A negative-control protein, bovine serum albumin, also showed no significant difference in its fractionation pattern in the presence versus absence of rVP2 (data not shown). This result indicates that, as expected, the 1 to 3 engineered alanine mutations had no observable effect on the overall capacity of rVP1 to bind to and be pulled down by rVP2 *in vitro*.

We next sought to confirm these rVP1-rVP2 binding results using a virus-like particle (VLP) encapsidation assay. Specifically, it is well known that when rVP2 is coexpressed along with rVP6 in Sf9 cells, VLPs will spontaneously assemble (14, 29, 30). If rVP1 is also coexpressed in the cells, it becomes encapsidated into the VLPs (via rVP2 binding) at stoichiometrically appropriate levels (i.e., a 1:10 ratio of rVP1 to rVP2) (30). To test whether the rVP1 mutants were still capable of being encapsidated into VLPs, Sf9 cells were infected with baculoviruses expressing simian strain SA11 rVP2 and rVP6, either in

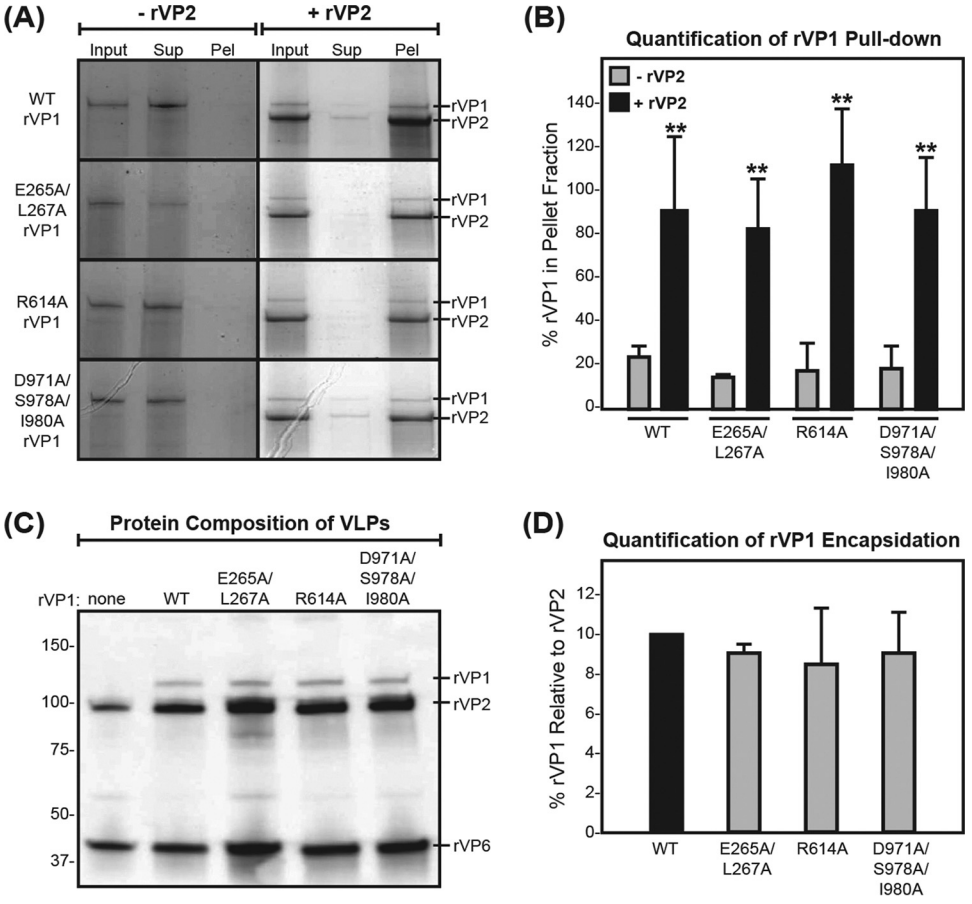

FIG 8 rVP2 binding capacity of loss-of-function rVP1 mutants. (A) Pulldown assay. WT or mutant rVP1 proteins were incubated in the absence (−) or presence (+) of rVP2. The input mixture was subjected to centrifugation to separate the supernatant (Sup) from the pellet (Pel) fractions. Samples were electrophoresed on a 10% SDS-polyacrylamide gel and visualized by Coomassie blue stain. (B) The percentage of rVP1 in the pellet fraction was quantified. Results are the means from >6 independent experiments using 2 protein batches. Error bars represent standard deviations from the mean. A double asterisk indicates a *P* value of <0.001. (C) rVP1 encapsidation assay. VLPs were generated in the absence of rVP1 (none) or in the presence of WT or mutant rVP1 proteins. Western blot analysis was performed to visualize the composition of purified VLPs. The locations of rVP1, rVP2, and rVP6 are shown. (D) The percentage of rVP1 relative to rVP2 was quantified. Results are the means from 3 independent experiments using 2 VLP batches. Error bars represent standard deviations from the mean.

the absence of rVP1 or in the presence of WT rVP1 or mutant rVP1 (E265A/L267A, R164A, or D971A/S978A/I980A). VLPs were purified using isopycnic centrifugation in cesium chloride, and their protein composition was analyzed by SDS-PAGE and silver staining (not shown) or by Western blotting using polyclonal antisera against VP1, VP2, and VP6 (Fig. 8C). The results show the presence of a 125-kDa band (i.e., rVP1) only in the VLPs generated with rVP1 coexpression, demonstrating polymerase encapsidation (Fig. 8C). There was no significant difference in the amounts of mutant rVP1 (relative to rVP2) and the WT control, which was set at 10% (Fig. 8D). This result confirms that of the pulldown assay and suggests that the rVP1 alanine mutants with loss-of-function phenotypes (i.e., E265A/L267A, R164A, and D971A/S978A/I980A) still retain their overall folding as well as their capacity to bind rVP2. It is most likely that the mutant rVP1 proteins are able to engage rVP2 via their nonmutated contact sites.

Loss-of-function rVP1 mutants show no major structural or dynamical changes *in silico*. We next performed unrestrained molecular dynamics simulations to gain insight into possible subtle conformational changes that could account for the loss-of-function phenotypes of rVP1 mutants in a manner that is independent of rVP2-induced activation. The structures of WT VP1 and homology models of E265A/L267A, R614A VP1, and D971A/S978A/I980A VP1 were each simulated for 20 ns at 300 K to

approximate the conditions of the *in vitro* dsRNA synthesis assay. We found no significant differences in the radius of gyration, the overall secondary structure content, or the overall root mean square deviation (RMSD) values for WT VP1 versus mutant VP1 proteins (Fig. 9A and data not shown). These results suggests that the alanine mutations did not induce globally destabilizing effects on the polymerase.

To identify putative locally destabilizing impacts and more modest structural and dynamical changes, root mean square fluctuations (RMSFs) of the α-carbons (WT VP1 versus mutant VP1) were used to calculate B-factors for each residue (Fig. 9B and C). The most extreme differences were detected in a modeled flexible surface-exposed loop (strain SA11 aa 346 to 358) of the PD (31). Specifically, residues 347, 349, and 352 were predicted to have reduced dynamical movement for all of the alanine mutants compared to WT VP1. This loop element was resolved in the recent *in situ* structure of actively transcribing DLPs and does not play any obvious role in catalysis (13). In a comparison of the mutants to each other, there were no significant differences in the movement of this loop, yet the mutants show phenotypic differences from each other *in vitro* (i.e., activities in decreasing order of E265A/L267A, R614A, and D971A/S978A/I980A) (Fig. 3, 5, and 6). Thus, the extent of loop movement does not correlate with *in vitro* functions of the rVP1 mutants.

Subtle dynamical differences were seen for various rVP1 mutants at other positions in the polymerase, including (i) NTD residues 1, 78, 156, and 157, (ii) finger subdomain residue 434, and (iii) CTD residues 723, 792 to 796, 819 and 820, and 849 (Fig. 9C). None of these sites are predicted to be directly involved in catalysis or in +RNA template recognition (13, 22, 27, 28). Thus, *in silico* analyses predict only subtle changes in the movement of the polymerase; we think these changes are unlikely to account for the loss-of-function phenotype of the rVP1 proteins in the *in vitro* dsRNA synthesis assay. Instead, we hypothesize that subtle loss of rVP2 contact at these sites reduced rVP1 enzymatic activation.

DISCUSSION

Rotavirus RNA synthesis is catalyzed by the VP1 polymerase and occurs within the confines of subviral particles (3, 4). Specifically, transcription of +RNAs occurs within DLPs, while replication of the dsRNA genome occurs within assembly intermediates. VP2 is critical for VP1-mediated dsRNA synthesis *in vitro* and *in vivo*; yet, the mechanism by which the core shell protein triggers polymerase function remains poorly understood (7–9, 14–20). Unfortunately, no structural information exists for the assembly intermediates, so the mode of VP1-VP2 interaction during dsRNA is not known. However, high-resolution structures of transcriptionally competent DLPs provide deep insight into the mode of VP1-VP2 binding during +RNA synthesis, which might be similar to that occurring during dsRNA synthesis (12, 13). These structures show that the surface of VP1 around the +RNA exit tunnel is contacted by the VP2 principal scaffold domain at 5 distinct sites (C1 to C5). In this study, we employed an *in vitro* dsRNA synthesis assay and a loss-of-function alanine mutagenesis approach to investigate which, if any, of the VP2 contact sites on VP1 that were revealed via structural analysis of DLPs (C1 to C5) are important for polymerase activity.

Our results show that alanine mutagenesis of residues within VP2 contact sites C2 (aa 547 to 550) and C5 (aa 1022 to 1025) had no effect on the capacity of rVP1 to synthesize dsRNA *in vitro* in the presence of rVP2 (Fig. 4 and 7). Residues within C2 are generally conserved across rotavirus strains and contain mostly polar residues with one hydrophobic residue in the middle (Fig. 4A). Although some residues within C2 have outward-facing side chains that neighbor the core shell, they do not directly clash with any of the VP2 monomers in the DLP structures (Fig. 4A) (12, 13). Alanine point mutations at each individual amino acid residue yielded mutants that synthesized dsRNA at levels that were indistinguishable from those of the WT rVP1 (Fig. 4C and D). It is possible that these C2 residues act in combination, and future multipoint mutagenesis across this region may be required. In contrast, for C5, we tested rVP1 mutants with two or three consecutive alanine mutations, including an obtrusive lysine-to-alanine substitution

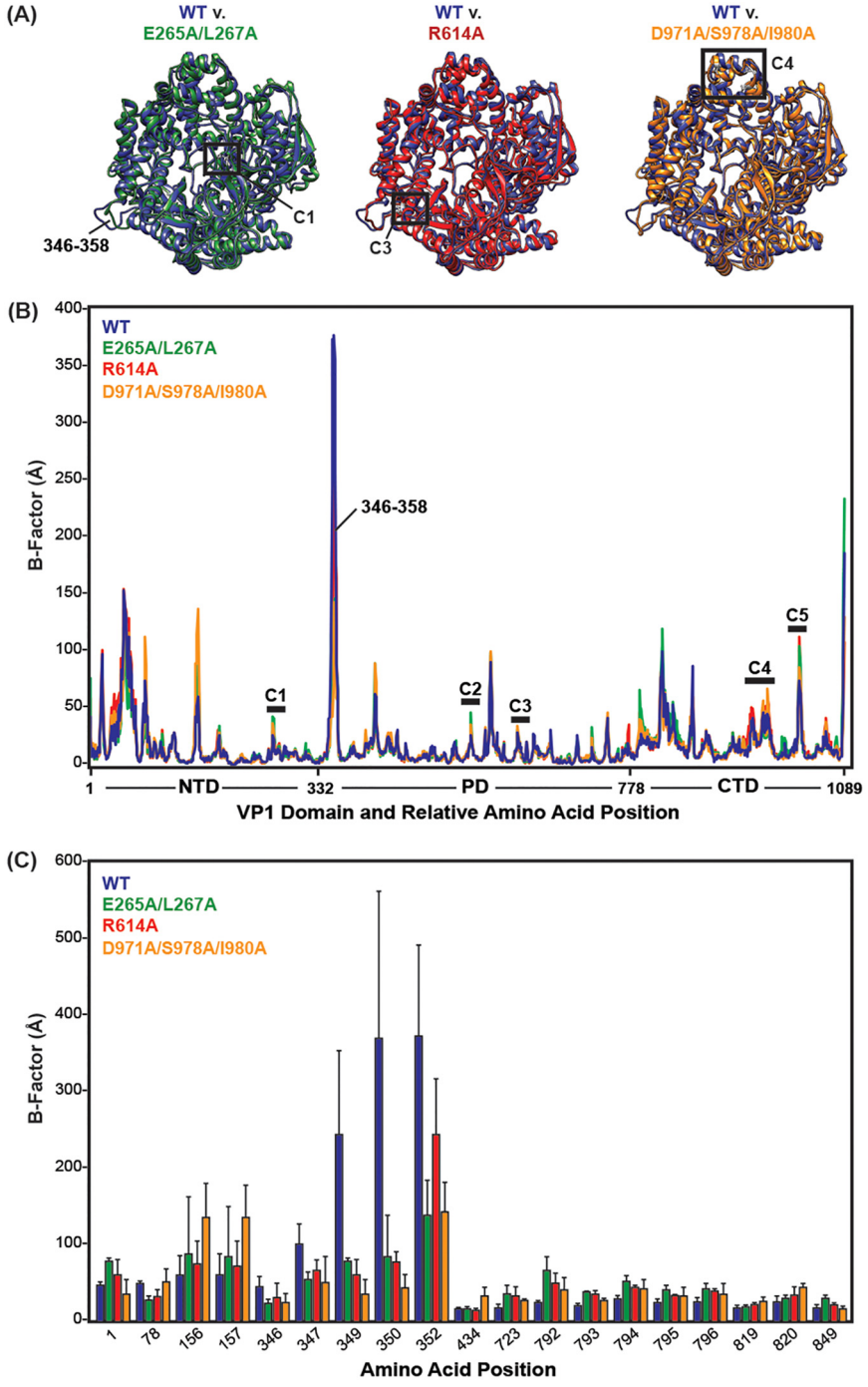

FIG 9 *In silico* molecular dynamics simulations of rVP1 loss-of-function mutants. Molecular dynamics simulations of VP1 protein structures. (A) Structure of WT VP1 (PDB accession no. 2R7R; blue) with final trajectory models of each loss-of-function mutant overlaid, as follows: E265A/L267A (green), R614A (red), and D971A/D978A/I980A (orange). The modeled loop (residues 346 to 358) is indicated in the left image, and the locations of C1, C3, and C4 are indicated for each mutant. The view of VP1 is from the front, similar to that shown in Fig. 2B (right). B-factors for each residue were calculated from the RMSF values of three trajectories. Average B-factors are shown for the entire VP1 proteins (B) or for sites of differentiation (C). (B and C) Residue position numbers are shown on the *x* axis. WT VP1 values are plotted in blue, E265A/L267A is plotted in green, R614A is plotted in red, and D971A/D978A/I980A is plotted in orange. Error bars represent standard deviations from the means following three independent trajectories. The modeled loop (residues 346 to 358) and the locations of C1, C3, and C4 are indicated in panel B.

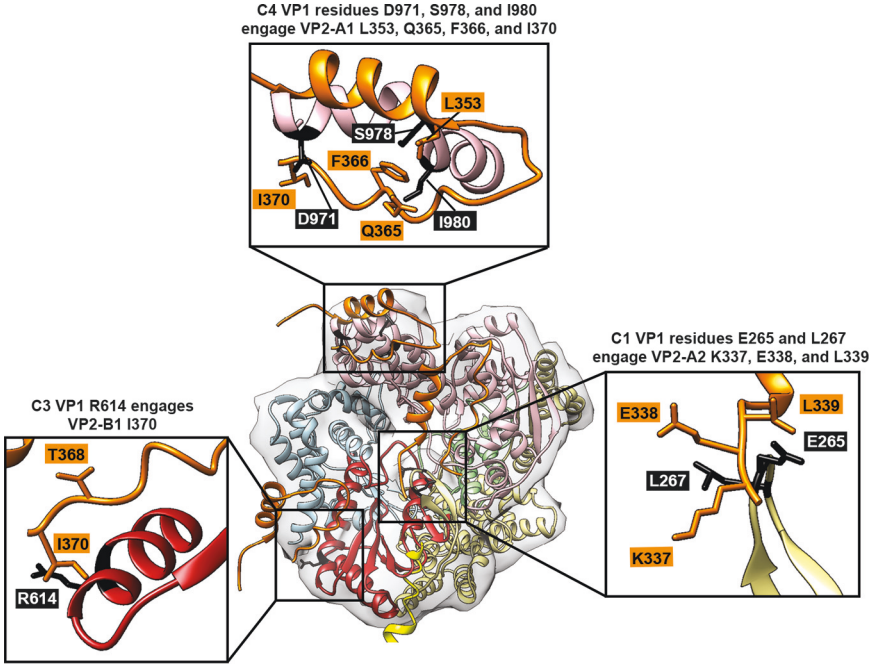

FIG 10 Core shell contact sites important for polymerase activity. (A) A ribbon drawing of VP1 (PDB accession no. 4AU6 and 4F5X) is shown centrally in the same orientation and coloration as in Fig. 2C. Ribbon drawings of VP2 contact sites (aa 73 to 100 and 337 to 370) are shown in the same orientation and coloration as in Fig. 2E. Black boxes outline areas that are magnified in the central image. For clarity, some regions of VP1 and VP2 have been removed in the magnified images. Side chains of VP1 are shown in black for C1, C3, and C4 residues that showed loss of function when mutated to alanine and are labeled. Side chains of corresponding regions of VP2 that may be interacting with regions C1, C3, and C4 are labeled and shown in orange. C1 is presumed to interact with VP2-A2 (aa 337 to 339, KEL), C3 is presumed to interact with VP2-B1 (aa I370), and C4 is presumed to interact with VP2-A1 (aa L353, Q365, F366, and I370).

(Fig. 7A). Several C5 residues contain long amino acid side chains that extend toward the VP2 core shell and directly clash with VP2. The observation that none of the mutations within C5 affect rVP1 functionality in the *in vitro* dsRNA synthesis assays strongly suggests that this region is not involved in rVP1 activation (Fig. 7C and D).

In contrast to sites C2 and C5, our results show that mutagenesis of some, but not all, residues within VP2 contact sites C1 (aa 264 to 267), C3 (aa 614 to 620), and C4 (aa 968 to 980) diminishes the capacity of rVP1 to synthesize dsRNA *in vitro* in the presence of rVP2 (Fig. 3, 5, and 6). Site C1 is located within the VP1 NTD and presumed to interact with VP2-A2 aa K337, E338, and L339 (Fig. 10). A glutamic acid-to-alanine (E265A) mutation within C1 was sufficient to reduce rVP1 activity only when it was combined with a more modest, leucine-to-alanine mutation (i.e., E265A/L267A) (Fig. 3C and D). This result suggests that either L267 is more important for rVP1 activation than E265 or that these residues work in combination. Future experiments will resolve the individual contributions of these residues. Another site that showed loss-of-function effects was site C3, which is located within the palm subdomain of the polymerase. While C3 does not directly clash with VP2 in the DLP structure, it is proximal to core shell protein residues 337 to 373 (Fig. 5A). A single R614A mutation within C3 significantly reduced dsRNA synthesis by VP1 (Fig. 5C and D). In particular, R614 is very close to residue I370 of the VP2-B1 monomer and may participate in an interaction (Fig. 10). In the future, it will be interesting to test whether the charged nature of R614 is critical for its robust activity. Still, the most dramatic effect on rVP2-dependent rVP1 activity was seen when mutations were engineered in site C4, which is located in the VP1 CTD. In particular, simultaneous alanine mutation at sites D971, S978, and I980 nearly ablated rVP1 functionality *in vitro* (Fig. 6A). These polymerase residues are located on the same side of an α-helix that engages VP2-A1 residues L353, Q365, F366, and I370 (Fig. 10) (12, 13).

Although there are several electrically charged residues within C4, D971 is interesting because the aspartic acid is highly conserved in group A rotavirus strains, and the amino acid side chain extends outward toward the VP2 core shell, contacting I370 (Fig. 6A). Unfortunately, the D971A single mutant did not express/fold properly and was therefore not amenable to enzyme assays. Nevertheless, the result that the double alanine mutant (S978A/I980A) showed levels of activity comparable to that of WT rVP1, but that the triple mutant (D971A/S978A/I980A) was significantly reduced in activity, suggests an important role for D971 (Fig. 6C). Alternatively, it is possible that these residues act in combination to mediate rVP1 activation. We are particularly intrigued about the notion that C4 mediates the core shell-induced activation of the polymerase because it contains numerous amino acid residues flanking D971 that are divergent in a comparison of the sequences from mammalian versus avian strains (Fig. 6A). Our previous results demonstrated that group A mammalian rotavirus rVP1 proteins (strains SA11, Wa, DS-1, and ETD) differ from group A avian rotavirus rVP1 (strain PO-13) in terms of their rVP2 activation specificities (18, 19). Thus, it is expected that there will be some mammalian versus avian sequence variation in the region of VP1 that is contacted by VP2 for enzyme activation.

It is important to note that mutations within C1, C3, and C4 residues of VP1 are predicted to decrease interaction(s) with VP2 that lead to enzyme activation, but they are not expected to ablate the overall capacity of these proteins to interact with each other. Indeed, the VP2 principal scaffold domain makes 5 large surface contacts with VP1 involving >30 amino acid residues. The flexible VP2 NTD makes additional known contacts with VP1 (via >10 additional residues outside the +RNA exit tunnel interface) (13). The contacts between the nonresolved portion of the VP2 NTD and VP1 are not known, but these flexible VP2 tethers are predicted to wrap around the entire polymerase and secure it against the scaffold domain (13). Thus, mutagenesis of 1 to 3 of the >40 contact residues between VP1 and VP2 would not be expected to ablate their interaction. This idea is consistent with our result that alanine E265A/L267A, R614A, and D971A/S978A/I980A mutants were still able to interact with rVP2 in pulldown and VLP encapsidation assays (Fig. 8). We posit that these other "nonactivational" VP2 binding events may simply function to ensure polymerase packaging into nascent particles during assembly or serve to tether the polymerase to the intraparticle framework. We expect that the loss-of-function rVP1 alanine mutants have lower rVP2 binding affinities only at their mutated contact sites. Future experiments seeking to test this notion will require the engineering of soluble, activatable rVP2 preparations.

At this time, we cannot fully exclude the possibility that the loss-of-function rVP1 alanine mutants have reduced polymerase activity due to factors that are independent of rVP2 binding. For instance, the mutations could have abrogated +RNA template binding, or they could have prevented the intramolecular structural changes that are requisite for polymerase activation. However, the engineered mutations are at surface-exposed sites, and they do not affect the overall folding of the proteins *in vitro* or *in silico*. In fact, molecular dynamics simulations reveal only subtle changes in movement at positions that are not known to be involved in catalysis or template binding (Fig. 9). Ongoing and future biochemical and computational experiments in our laboratory will more fully characterize the rVP1 mutants generated in this study, as well as create additional mutants (including on the rVP2 side) to probe the importance of the core shell contact sites during dsRNA synthesis. Nevertheless, the results presented here are an important first step toward unraveling the complex intraparticle RNA synthesis mechanism of rotavirus.

MATERIALS AND METHODS

Generation of rVP1- and rVP2-expressing baculoviruses. To create pENTR-1A entry vectors for the generation of baculoviruses expressing single- and multipoint rVP1 mutants, outward PCR and site-directed mutagenesis were performed. In all PCRs, Accuprime *Pfx* Supermix (Invitrogen) was used as the enzyme, and the sequence was amplified using 5′-phosphorylated primers and pENTR-1A-SA11 VP1 as the template (17). Mutagenic primer sequences are available upon request. PCRs were treated with DpnI (New England BioLabs) to remove methylated template, and cDNAs were gel purified prior to ligation

using T4 DNA ligase (New England BioLabs). To create an entry vector for the expression of SA11 rVP2, the cDNA was codon optimized for expression in Sf9 insect cells, synthesized *de novo* by GeneArt (Regensburg, Germany), and subcloned into pENTR-1A. The amino acid sequence of SA11 rVP2 protein directly matches the sequence in the GenBank database (accession no. DQ838631). All final pENTR-1A entry vector clones were sequenced across the rVP1- or rVP2-coding regions prior to the generation of baculoviruses.

The BaculoDirect expression system (Life Technologies) was used in accordance with the manufacturer's protocol to create recombinant baculoviruses expressing rVP1 or rVP2. Briefly, the rVP1- and rVP2-encoding genes in the pENTR-1A entry vectors were individually inserted into BaculoDirect C-Term linear DNA by recombination with LR Clonase II. The baculovirus DNA was then transfected into *Spodoptera frugiperda* (Sf9) cells using Cellfectin reagent (Life Technologies), and recombinant baculovirus was harvested from selective medium containing 100 μM ganciclovir. Sf9 cells were maintained at 28°C in complete Grace's medium (Life Technologies) supplemented to contain 10% fetal bovine serum, 100 U/ml penicillin, 100 μg/ml streptomycin, 0.5 μg/ml amphotericin B, and 1% Pluronic F-68 (Life Technologies). The baculovirus expressing wild-type SA11 rVP1 was generated previously (17).

Purification of rVP1 and rVP2 and *in vitro* dsRNA synthesis assays. His-tagged rVP1 and untagged rVP2 proteins were expressed and purified as described previously (18). Purified rVP1 and rVP2 proteins were maintained at 4°C in low-salt buffer (2 mM Tris-HCl [pH 7.5], 0.5 mM EDTA, 0.5 mM dithiothreitol) until their use, and they were assessed for quality and relative quantity versus Precision Plus protein kaleidoscope prestained protein standards (Bio-Rad) in 10% SDS-PAGE gels (Protean) and with Coomassie blue staining (Thermo Scientific). *In vitro* replicase synthesis assays were performed as described previously (17–19). Briefly, each 20-μl reaction mixture contained 2 pmol rVP1, 8 pmol rVP2, 8 pmol SA11 gene 8 +RNA, 50 mM Tris-HCl (pH 7.5), 1 μl of 30% polyethylene glycol 8000, 20 mM magnesium acetate, 1.6 mM manganese acetate, 2.5 mM dithiothreitol, 1.25 mM (each) ATP, CTP, and UTP, 5 mM GTP, 1 μl RNasin (Promega), and 1 μCi [^{32}P]UTP (3,000 Ci/mmol; PerkinElmer). Reactions proceeded at 37°C for 3 h. The ^{32}P-labeled dsRNA products of the reaction were electrophoresed in 4 to 15% SDS-PAGE gels (Protean) and visualized using a GE Healthcare Storm 860 phosphorimager. A minimum of 2 replicate experiments were performed from 3 to 4 batches of independently purified recombinant proteins ($n = 6$ to 8 replicates total). Quantification of images obtained using the phosphorimager was completed using ImageQuant 5.2 software or ImageJ 2.0v. One-sample *t* tests of the mean were performed for each data set using Smith's Statistical Package 2.80v. *P* values of <0.005, in comparison to the 100% set value of wild-type SA11 rVP1, were considered statistically significant.

rVP1-rVP2 pulldown assays. To assess the overall rVP1-rVP2 protein binding capacity, a pulldown assay was performed. Specifically, 60-μl reaction mixtures containing 4 pmol WT rVP1 or each loss-of-function mutant rVP1 (i.e., E265A/L267A, R614A, and D971A/S978A/I980A mutants) were combined with 16 pmol rVP2 (or no rVP2 as a control). Reaction volumes were normalized with low-salt buffer (2 mM Tris-HCl [pH 7.5], 0.5 mM EDTA, 0.5 mM dithiothreitol). Reactions incubated for 5 min at 28°C to allow binding, and then an aliquot was removed to assess input protein amounts. Reaction mixtures were then subjected to centrifugation at 16,000 $\times$ *g* for 5 min at 4°C to pellet rVP2. The supernatant fraction was transferred to a new tube, whereas the pellet fraction was resuspended in an equivalent volume of low-salt buffer. Equal-volume samples (~20 μl) were assessed for relative quantity in 10% SDS-PAGE gels (Protean) and Coomassie blue staining (Thermo Scientific). A minimum of 3 replicate experiments were performed from 2 batches of independently purified recombinant proteins. ImageJ 2.0v was used to quantify the amount of rVP1 in the pellet fractions in the presence versus absence of rVP2. One-sample *t* tests of the mean were performed for each data set using Smith's Statistical Package 2.80v, with *P* values of <0.001 considered significant.

rVP1 encapsidation into VLPs. As an additional test of rVP1-rVP2 binding, strain SA11 VLPs were generated as described by Boudreaux et al. (30). Control VLPs were generated by Sf9 cell expression of rVP2 and rVP6 in the absence of rVP1, whereas polymerase encapsidation was tested by coexpression of either WT rVP1 or each loss-of-function mutant rVP1 (E265A/L267A, R614A, and D971A/S978A/I980A mutants). Briefly, VLPs that were released into the medium following a 5-day baculovirus infection were first concentrated by pelleting through a 35% (wt/vol) sucrose cushion in TNE buffer (20 mM Tris [pH 7.4], 50 mM NaCl, 1 mM EDTA) for 1.5 h at 80,000 $\times$ *g* and 4°C. The protein pellet was resuspended in TNE buffer containing complete protease inhibitor tablets (Roche), and VLPs were further purified by isopycnic centrifugation in cesium chloride (density, 1.28 to 1.31 g/cm^3) for 16 h at 110,000 $\times$ *g* and 12°C. Visible protein bands were collected in 500-ml fractions from each gradient and repelleted at 1.5 h at 80,000 $\times$ *g* and 4°C. Approximately 400 ng of each purified VLP preparation was electrophoresed in 10% SDS-polyacrylamide gels and stained using the SilverQuest kit (Thermo Fisher) or transferred to nitrocellulose membranes for Western blot analysis. Guinea pig polyclonal antibodies anti-VP1/anti-VP2 and anti-VP6 were generously provided by John Patton (Indiana University) and used at a 1:1,000 dilution. Goat anti-guinea pig-horseradish peroxidase (pig-HRP) secondary antibodies (Thermo Fisher) were used at a 1:10,000 dilution. Western blots were developed using SuperSignal West Pico Plus chemiluminescent substrate (Thermo Fisher) and imaged using an Amersham Imager 600. A minimum of 3 replicate gels were analyzed from 2 batches of independently purified VLPs. ImageJ 2.0v was used to quantify the amount of rVP1 relative to rVP2. One-sample *t* tests of the mean were performed for each data set using Smith's Statistical Package 2.80v, with WT rVP1 being set at 10% and rVP2 at 100%.

Visual analyses of VP1 sequence variation and structure. Several representative full-length amino acid sequences were obtained from the NCBI (https://www.ncbi.nlm.nih.gov/nuccore), including those of simian strains SA11 (accession no. AFK09589) and RRV (accession no. ACC94312), human strains DS-1 (accession no. AEG25322), Wa (accession no. AFR77806), and AU-1 (accession no. ABF67540), bovine

strains UK (accession no. P21615) and RF (accession no. P17468), murine strain ETD (accession no. AEA30040), and avian strain PO-13 (accession no. BAA24146). Amino acid alignments were created using Geneious Pro v10.2.3 (Biomatters) and the BLOSUM matrix of the ClustalW algorithm. Structure images were generated using UCSF Chimera molecular modeling system v1.13 and PDB files 4AU6 and 4F5X (12, 22, 32).

***In silico* molecular dynamics simulations.** Molecular dynamics simulations were performed using the program GROMACS 2018 on a modified atomic model of VP1 (PDB accession no. 2R7Q), described by McKell et al. (22, 31). The UCSF Chimera software program was used for all visualizations and to generate mutants with Chimera's Rotamers tool, as previously described (32). Structures were solvated with a three-point water model (SPC/E) in an explicit rhombic dodecahedron water box (solute-box distance of 1.0 nm) under periodic boundary conditions, with charges neutralized by chloride ions (33, 34). The AMBER99SB-ILDN force field was used for all simulations (35). Starting structures were energy minimized until convergence at a maximum force (F_{max}) of $<$1,000 kJ/mol/nm. A 100-ps position-restrained NVT equilibration simulation was run for water relaxation at 300 K using a modified Berendsen (velocity rescaling) thermostat, followed by a 100-ps NPT equilibration simulation using the Parrinello-Rahman barostat for pressure coupling. After equilibration, an unrestrained 20-ns NPT molecular dynamics simulation was run. Three trajectories initiated with different random seeds were run for each protein structure.

Trajectories were postprocessed to correct for periodicity. The root mean square fluctuation (RMSF) of all α-carbons from each of the three trajectories was calculated using the gmx rmsf command in GROMACS. B-factors for each residue were calculated from the RMSF values using the equation B-factor $= (8\Pi^2/3) \times (\text{RMSF})^2$. The first 5 ns of each trajectory for each protein variant was trimmed, and the three trajectories were then concatenated in GROMACS. A cluster analysis was performed on each concatenated trajectory with a cutoff of 0.125 nm using the gromos algorithm to allow examination of the structures most populated in the MD simulations (36). The root mean square deviation (RMSD) of the protein backbone from the starting structure and radius of gyration were calculated using the GROMACS rms and gyrate commands, respectively, for each time point on the concatenated trajectories. The GROMACS command do_dssp was used to run the dssp program to calculate the secondary structure for each time point of the concatenated trajectories (37, 38); analysis of the dssp output was done using ss_analysis.py written by João Henriques (https://gist.github.com/jmhenriques/9a531bce9d5f549d53a5).

ACKNOWLEDGMENTS

We thank current and former members of the McDonald laboratory for intellectual and technical support. We also thank John Patton for providing guinea pig polyclonal antisera.

This work was supported through funding from the Virginia Tech Carilion Research Institute and Wake Forest University and through a grant from the National Institutes of Health (R01-AI116815). C.L.S. was also supported by the Graduate Program in Translational Biology, Medicine and Health at Virginia Tech.

REFERENCES

1. Tate JE, Burton AH, Boschi-Pinto C, Parashar UD, World Health Organization-Coordinated Global Rotavirus Surveillance Network. 2016. Global, regional, and national estimates of rotavirus mortality in children <5 years of age, 2000–2013. Clin Infect Dis 62(Suppl 2):S96–S105. https://doi.org/10.1093/cid/civ1013.
2. Estes MK, Kapikian AZ. 2006. Rotaviruses and their replication. *In* Knipe DM, Howley PM (ed), Fields virology, 5th ed. Lippincott Williams & Wilkins, Philadelphia, PA.
3. Trask SD, McDonald SM, Patton JT. 2012. Structural insights into the coupling of virion assembly and rotavirus replication. Nat Rev Microbiol 10:165–177. https://doi.org/10.1038/nrmicro2673.
4. Trask SD, Ogden KM, Patton JT. 2012. Interactions among capsid proteins orchestrate rotavirus particle functions. Curr Opin Virol 2:373–379. https://doi.org/10.1016/j.coviro.2012.04.005.
5. Lawton JA, Estes MK, Prasad BV. 2000. Mechanism of genome transcription in segmented dsRNA viruses. Adv Virus Res 55:185–229. https://doi.org/10.1016/S0065-3527(00)55004-0.
6. Lawton JA, Estes MK, Prasad BV. 1997. Three-dimensional visualization of mRNA release from actively transcribing rotavirus particles. Nat Struct Biol 4:118–121. https://doi.org/10.1038/nsb0297-118.
7. Patton JT, Gallegos CO. 1988. Structure and protein composition of the rotavirus replicase particle. Virology 166:358–365. https://doi.org/10.1016/0042-6822(88)90506-5.
8. Gallegos CO, Patton JT. 1989. Characterization of rotavirus replication intermediates: a model for the assembly of single-shelled particles. Virology 172:616–627. https://doi.org/10.1016/0042-6822(89)90204-3.
9. Boudreaux CE, Kelly DF, McDonald SM. 2015. Electron microscopic analysis of rotavirus assembly-replication intermediates. Virology 477:32–41. https://doi.org/10.1016/j.virol.2015.01.003.
10. Prasad BV, Rothnagel R, Zeng CQ, Jakana J, Lawton JA, Chiu W, Estes MK. 1996. Visualization of ordered genomic RNA and localization of transcriptional complexes in rotavirus. Nature 382:471–473. https://doi.org/10.1038/382471a0.
11. McClain B, Settembre E, Temple BR, Bellamy AR, Harrison SC. 2010. X-ray crystal structure of the rotavirus inner capsid particle at 3.8 Å resolution. J Mol Biol 397:587–599. https://doi.org/10.1016/j.jmb.2010.01.055.
12. Estrozi LF, Settembre EC, Goret G, McClain B, Zhang X, Chen JZ, Grigorieff N, Harrison SC. 2013. Location of the dsRNA-dependent polymerase, VP1, in rotavirus particles. J Mol Biol 425:124–132. https://doi.org/10.1016/j.jmb.2012.10.011.
13. Ding K, Celma CC, Zhang X, Chang T, Shen W, Atanasov I, Roy P, Zhou ZH. 2019. In situ structures of rotavirus polymerase in action and mechanism of mRNA transcription and release. Nat Commun 10:2216. https://doi.org/10.1038/s41467-019-10236-7.
14. Zeng CQ, Wentz MJ, Cohen J, Estes MK, Ramig RF. 1996. Characterization and replicase activity of double-layered and single-layered rotavirus-like particles expressed from baculovirus recombinants. J Virol 70:2736–2742.
15. Patton JT. 1996. Rotavirus VP1 alone specifically binds to the 3′ end of viral mRNA, but the interaction is not sufficient to initiate minus-strand synthesis. J Virol 70:7940–7947.
16. Tortorici MA, Broering TJ, Nibert ML, Patton JT. 2003. Template recognition and formation of initiation complexes by the replicase of a

segmented double-stranded RNA virus. J Biol Chem 278:32673–32682. https://doi.org/10.1074/jbc.M305358200.
17. McDonald SM, Aguayo D, Gonzalez-Nilo FD, Patton JT. 2009. Shared and group-specific features of the rotavirus RNA polymerase reveal potential determinants of gene reassortment restriction. J Virol 83:6135–6148. https://doi.org/10.1128/JVI.00409-09.
18. McDonald SM, Patton JT. 2011. Rotavirus VP2 core shell regions critical for viral polymerase activation. J Virol 85:3095–3105. https://doi.org/10.1128/JVI.02360-10.
19. Steger CL, Boudreaux CE, LaConte LE, Pease JB, McDonald SM. 2018. Group A rotavirus VP1 polymerase and VP2 core shell proteins: intergenotypic sequence variation and in vitro functional compatibility. J Virol 93:e01642-18. https://doi.org/10.1128/JVI.01642-18.
20. Long CP, McDonald SM. 2017. Rotavirus genome replication: some assembly required. PLoS Pathog 13:e1006242. https://doi.org/10.1371/journal.ppat.1006242.
21. Zeng CQ, Labbé M, Cohen J, Prasad BV, Chen D, Ramig RF, Estes MK. 1994. Characterization of rotavirus VP2 particles. Virology 15:55–65. https://doi.org/10.1006/viro.1994.1265.
22. Lu X, McDonald SM, Tortorici MA, Tao YJ, Vasquez-Del Carpio R, Nibert ML, Patton JT, Harrison SC. 2008. Mechanism for coordinated RNA packaging and genome replication by rotavirus polymerase VP1. Structure 16:1678–1688. https://doi.org/10.1016/j.str.2008.09.006.
23. McDonald SM, Tao YJ, Patton JT. 2009. The ins and outs of four-tunneled Reoviridae RNA-dependent RNA polymerases. Curr Opin Struct Biol 19:775–782. https://doi.org/10.1016/j.sbi.2009.10.007.
24. McDonald SM. 2013. RNA synthetic mechanisms employed by diverse families of RNA viruses. Wiley Interdiscip Rev RNA 4:351–367. https://doi.org/10.1002/wrna.1164.
25. Zhang X, Ding K, Yu X, Chang W, Sun J, Zhou ZH. 2015. In situ structures of the segmented genome and RNA polymerase complex inside a dsRNA virus. Nature 527:531–534. https://doi.org/10.1038/nature15767.
26. Ding K, Nguyen L, Zhou ZH. 2018. In situ structures of the polymerase complex and RNA genome show how aquareovirus transcription machineries respond to uncoating. J Virol 92:e00774-18. https://doi.org/10.1128/JVI.00774-18.
27. Ogden KM, Ramanathan HN, Patton JT. 2011. Residues of the rotavirus RNA-dependent RNA polymerase template entry tunnel that mediate RNA recognition and genome replication. J Virol 85:1958–1969. https://doi.org/10.1128/JVI.01689-10.
28. Ogden KM, Ramanathan HN, Patton JT. 2012. Mutational analysis of residues involved in nucleotide and divalent cation stabilization in the rotavirus RNA-dependent RNA polymerase catalytic pocket. Virology 431:12–20. https://doi.org/10.1016/j.virol.2012.05.009.
29. Zeng CQ, Estes MK, Charpilienne A, Cohen J. 1998. The N terminus of rotavirus VP2 is necessary for encapsidation of VP1 and VP3. J Virol 72:201–208.
30. Boudreaux CE, Vile DC, Gilmore BL, Tanner JR, Kelly DF, McDonald SM. 2013. Rotaviruscore shell subdomains involved in polymerase encapsidation into virus-like particles. J Gen Virol 94:1818–1826. https://doi.org/10.1099/vir.0.052951-0.
31. McKell AO, LaConte LEW, McDonald SM. 2017. A temperature-sensitive lesion in the N-terminal domain of the rotavirus polymerase affects its intracellular localization and enzymatic activity. J Virol 91:e00062-17. https://doi.org/10.1128/JVI.00062-17.
32. Pettersen EF, Goddard TD, Huang CC, Couch GS, Greenblatt DM, Meng EC, Ferrin TE. 2004. UCSF Chimera—a visualization system for exploratory research and analysis. J Comput Chem 25:1605–1612. https://doi.org/10.1002/jcc.20084.
33. Abraham MJ, Murtola T, Schulz R, Páll S, Smith JC, Hess B, Lindahl E. 2015. GRO-MACS: high performance molecular simulations through multi-level parallelism from lap-tops to supercomputers. SoftwareX 1–2:19–25. https://doi.org/10.1016/j.softx.2015.06.001.
34. Berendsen HJC, Grigera JR, Straatsma TP. 1987. The missing term in effective pair potentials. J Phys Chem 91:6269–6271. https://doi.org/10.1021/j100308a038.
35. Lindorff-Larsen K, Piana S, Palmo K, Maragakis P, Klepeis JL, Dror RO, Shaw DE. 2010. Improved side-chain torsion potentials for the Amber ff99SB protein force field. Proteins 78:1950–1958. https://doi.org/10.1002/prot.22711.
36. Daura X, Gademann K, Jaun B, Seebach D, van Gunsteren WF, Mark AE. 1999. Peptide folding: when simulation meets experiment. Angew Chem Int Ed 38:236–240. https://doi.org/10.1002/(SICI)1521-3773(19990115)38:1/2<236::AID-ANIE236>3.3.CO;2-D.
37. Kabsch W, Sander C. 1983. Dictionary of protein secondary structure: pattern recognition of hydrogen-bonded and geometrical features. Biopolymers 22:2577–2637. https://doi.org/10.1002/bip.360221211.
38. Touw WG, Baakman C, Black J, Te Beek TAH, Krieger E, Joosten RJ, Vriend G. 2015. A series of PDB related databases for everyday needs. Nucleic Acids Res 43:D364–D368. https://doi.org/10.1093/nar/gku1028.